van Gasselt *et al. Earth, Planets and Space* (2017) 69:35
DOI 10.1186/s40623-017-0620-8

Earth, Planets and Space

LETTER Open Access

The Oasis impact structure, Libya: geological characteristics from ALOS PALSAR-2 data interpretation

Stephan van Gasselt*, Jung Rack Kim, Yun-Soo Choi and Jaemyeong Kim

Abstract

Optical and infrared remote sensing may provide first-order clues for the identification of potential impact structures on the Earth. Despite the free availability of at least optical image data at highest resolution, research has shown that remote sensing analysis always remains inconclusive and extensive groundwork is needed for the confirmation of the impact origin of such structures. Commonly, optical image data and digital terrain models have been employed mainly for such remote sensing studies of impact structures. With the advent of imaging radar data, a few excursions have been made to also employ radar datasets. Despite its long use, capabilities of imaging radar for studying surface and subsurface structures have not been exploited quantitatively when applied for the identification and description of such features due to the inherent complexity of backscatter processes. In this work, we make use of higher-level derived radar datasets in order to gain clearer qualitative insights that help to describe and identify potential impact structures. We make use of high-resolution data products from the ALOS PALSAR-1 and ALOS PALSAR-2 L-band sensors to describe the heavily eroded Oasis impact structure located in the Libyan Desert. While amplitude radar data with single polarization have usually been utilized to accompany the suite of remote sensing datasets when interpreting impact structures in the past, we conclude that the integration of amplitude data with HH/HV/HH–HV polarization modes in standard and, in particular, in Ultra-Fine mode, as well as entropy–alpha decomposition data, significantly helps to identify and discriminate surface units based on their consolidation. Based on the overarching structural pattern, we determined the diameter of the eroded Oasis structure at 15.6 ± 0.5 km.

Keywords: DInSAR, Impact cratering, Oasis, Libya, Paleodrainage, Geomorphology, Remote sensing, ALOS PALSAR

Introduction and background

Remote sensing data analyses have advanced to an important and commonly utilized tool for the surface investigation and characterization of potential or already confirmed impact structures (e.g., Garvin et al. 1992; Wagner et al. 2002; Koeberl 2004; Koeberl et al. 2005a, b; Buchner and Schmieder 2007; Folco et al. 2010, 2011; Schmieder et al. 2008, 2013; Reimold and Koeberl 2014). They are often the only method to potentially identify new impact structures, in particular in areas of limited accessibility. However, not always has the application of remote sensing data analyses been rewarded with success, and the lack of diagnostic criteria has caused substantial debate in the past (e.g., Papagiannis 1989; Paillou et al. 2006a, b; El-Baz and Ghoneim 2007; Buchner and Schmieder 2007; Schmieder et al. 2008, 2013; Orti et al. 2008; Cigolini et al. 2012; Daneshvar 2015). Some of the false detections found—at least temporal—entry into the literature and databases, over which scientific debate ensued (see, e.g., discussion in Reimold 2007; Pati and Reimold 2007; Crósta and Reimold 2015). Despite their generally mega-scale size, impact structures are eventually identified on the level of microscales (e.g., French and Koeberl 2010; Reimold et al. 2013, 2014).

While most large bolide impacts, bar very low-angle impacts, produce quasi-circular crater forms when impacting on planetary surfaces, not all circular features are caused by impacts. The lack of clear diagnostic

*Correspondence: svangasselt16@uos.ac.kr
Department of Geoinformatics, University of Seoul, 163, Seoulsiripdae-ro, Seoul 02504, Korea

geomorphic or morphometric criteria in remote sensing data does not allow to consider impacts as a necessary requirement for the formation of such morphologies (e.g., Abels et al. 2000; Reimold and Koeberl 2014). On the usually densely cratered and vegetation-free surfaces of other terrestrial planets, the forward argumentation is sometimes reversed and usually convincing arguments need to be found *against* an impact origin (e.g., van Gasselt et al. 2007; Michaelski and Bleacher 2013). And even there, this might cause considerable debate despite the usually simple stratigraphic target environment and availability of super-resolution image data down to submeter scale from recent sensors on the Mars or Lunar Reconnaissance Orbiters.

The list of search criteria for detection of possible impact structures by remote sensing data analysis includes the presence of obvious and large-scale morphologies such as a sub-circular shape, remains of a potentially elevated rim or a central uplift or ring structures, and for higher-resolution data, target-specific shape criteria, drainage system layout, fault arrangements or target characteristic layering properties caused by the impact (e.g., Garvin et al. 1992; Abels et al. 2000; Koeberl 2004; Buchner and Schmieder 2007). Alternatively, either comparison with confirmed impact structures or exclusion from other morphologically similar features (Buchner and Schmieder 2007) provided additional criteria. Eventually, however, extensive field and laboratory work are required to confirm any initial detections of possible impact structures (e.g., Reimold et al. 2014; French and Koeberl 2010). It is thus evident that remote sensing image and hyperspectral data analysis and investigation of topographic characteristics only form the first step in building a case for confirmation of impact origin either by identifying potential structures or by establishing the context for detailed field analysis.

With the advent of radar data as a dataset additional to optical data, a powerful toolkit was provided for potential additional arguments about compositional and structural characteristics of the surface and the near subsurface independent of weather conditions and cloud coverage. The advantages of L-band radar imaging in arid regions were emphasized early in the literature (e.g., Elachi et al. 1984) when the detection of hidden subsurface structures by Shuttle Imaging Radar (SIR) made considerable scientific impact (McCauley et al. 1982; Schaber et al. 1986). Subsequent analyses made use of the Japanese *JERS-1* L-band radar in order to map the subsurface structure at resolutions down to 18 m/px. The JERS-1 dataset was qualitatively used to show some of the structural inventory of an alleged impact crater, and while it provided much more detail on the structural imprint when compared to optical image data, it did not add much to what was seen already in a SRTM-based terrain model (Paillou et al. 2003). The Canadian *Radarsat-1* SAR payload operating in the C-band at 5.3 GHz received wide interest during the last two decades, also for investigating the structure of eroded impact craters and the structural fingerprint and lithological settings (Abels et al. 2000; Smith et al. 2014).

Until 2013, *Radarsat-1* provided up to 10-m-resolution data in Fine mode. Resolutions of up to 1 m are obtained in Ultra-Fine mode for the *Radarsat-2* system launched in 2007 with full polarimetric data that have been used, also qualitatively, for impact crater investigations (Mader 2015). *Radarsat* and ESA's *ERS-1* amplitude data of the BP and Oasis structures were compared to optical data by Koeberl et al. (2005b), and it was found that the observed ring structures of the BP and Oasis impact craters were generally more pronounced in the radar data.

Our work is aimed at investigating the Oasis impact structure by making use of high-resolution *ALOS PALSAR-1* and *ALOS PALSAR-2* observations and derived data products. Multi-polarization amplitude image, phase coherence representations, as well as full polarimetric decomposition techniques complement the conventional SAR amplitude image data and are investigated in order to characterize Oasis' near-subsurface structure. Due to longer wavelength, L-band radar observations achieve greater penetration depths, which allows us to potentially map more subsurface features (e.g., Richards 2009: 152). We here demonstrate the potential use of performing a technically more complex data analysis and discuss potential benefit for the analysis of such landforms.

Geologic and geomorphologic settings

The Oasis impact structure is a highly eroded structure located in southeastern Libya at 24°24′E, 24°34′N, south of the BP impact crater (Fig. 1a, b; Kohman et al. 1967; Martin 1969; French et al. 1972; Koeberl et al. 2005b; Reimold and Koeberl 2014 and references therein). The diameter of the Oasis structure is still debated. Estimates have ranged from 5.1 to 11.5 km (French et al. 1974), 18 km (Koeberl et al. 2005b) or even up to 25–36 km (Gibson et al. 2011), variably based on fieldwork and remote sensing studies.

The age of Oasis is poorly constrained to less than 120 million years (e.g., Reimold and Koeberl 2014). The impact occurred into likely sub-horizontal sandstones and subordinate siltstones/shales of the Paleozoic Kufrah basin, specifically involving the lower Cretaceous Nubian Sandstone Formation (Reimold and Koeberl 2014). Today, the highly eroded structure comprises an inner ring with a diameter of approximately 5.1 km that is surrounded by a flat depression (Reimold and Koeberl 2014;

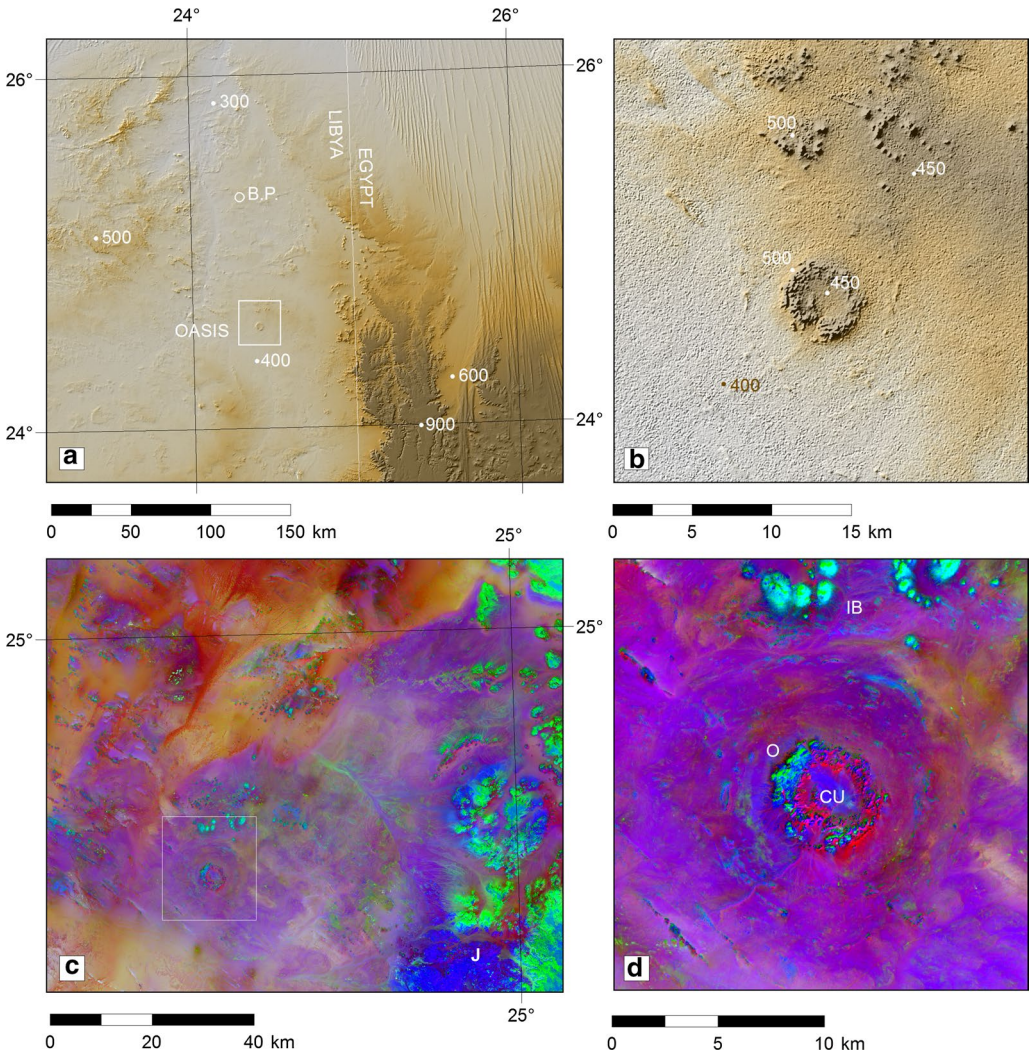

Fig. 1 **a** Location of the Oasis and BP impact structures in eastern Libya (GMTED at 240 m/px, colorized shaded relief) and **b** topographic setting of the Oasis impact crater (SRTM at 30 m/px, colorized shaded relief). **c** Landsat 8 ETM pan-sharpened PC representation with principal components 1–3 represented as RGB (15 m/px). Location of subfigure *d* marked by *white box*. **d** Same image basis with close-up of the Oasis impact structure, labels IB and IR refer to occurrences of inselbergs and remnants of the inner ring structure, respectively. The center of the impact structure is located at 24°24′E, 24°34′N

Fig. 1a–d).The topography reflects underlying lithology, and thus, the inner ring is mainly composed of relatively resistant sandstones, while the surrounding plains and the innermost depression are underlain by Carboniferous sediments (Reimold and Koeberl 2014; Gibson et al. 2011). Also, local hydrothermalism has been considered conceivable based on limited field sampling (Gibson et al. 2011).

Marine transgression caused by the Early Cretaceous opening of the Atlantic and basin subsidence as a consequence of the stress exerted on the African Plate caused deposition of massive sandstone deposits in the Kufrah basin (Pachur and Altmann 2006: 157). The basin is delimited to the south by the Ennedi Plateau and the Ouaddaï highlands as well as the southeastern Darfur Basin (Chad), toward the east by the Dakhla Basin in Egypt and toward the west and southwest by the Tibesti mountain plateau, which provided material for the basin fill. To the north, the Syrte basin connects the Kufrah Basin to the Mediterranean Sea (e.g., Pachur and Altmann 2006: 22). That connection has long been studied to investigate a mid-Miocene paleohydrological river network (Paillou et al. 2009, 2013; Griffin 2002, 2006; Pachur and Altmann 2006; Drake et al. 2008). The basin's paleohydrology played a major geomorphic role in the late Miocene when north Africa underwent the Messinian

Salinity Crisis (MSC) and the desiccation of the Mediterranean Sea caused formation of extensive valley networks and transport pathways toward the north and the southern Chad Basin (Barr and Walker 1973; Paillou et al. 2009).

Relatively recently, image data from the PALSAR sensor were used over the Libyan Desert to delineate buried fluvial features in more detail and discuss their extent toward the Mediterranean Sea (Paillou et al. 2009, 2013). This has extended work of the 1980s based on SIR and Landsat optical image data to delineate the paleoriver systems of the southern Dakhla basin to the east and the northern Dharfur basin to the south (McCauley et al. 1982).

Methods and data processing

Vegetation canopy and sedimentary deposits are the main barriers to detect and trace eroded and buried geomorphologic features. Remote sensing approaches in the optical and infrared wavelength domain provide only limited insights into such features for obvious reasons, and they can provide only indirect information about the subsurface if combined with topographic data. The SAR-based imaging potential to investigate surface and shallow subsurface structures has been noticed after Shuttle Imaging Radar (SIR) A to C imagery was successfully used to map geomorphic features over less vegetated topography (McHone et al. 2002). There has been a substantial amount of research work exploiting geometrical properties of surfaces including slope and roughness estimates using patterns and contrasts in SAR image tone and texture (e.g., Abdelsalam et al. 2000; Adams et al. 1981; Blom et al. 1984; Berlin et al. 1986; Grandjean et al. 2001; Paillou et al. 2006a, b). In particular, the potential of the low frequency domain (1–2 GHz) of L-band spaceborne SAR, when compared to applications of shorter wavelengths of C, S and X band SAR, is obvious for the purpose of subsurface mapping. This is mainly caused by larger penetration depth into the canopy or dry soils and the extensive coverage that enables monitoring of target areas.

With the deployment of spaceborne L-band SAR on the *Japanese Earth Resources Satellite (JERS)1* (Nemoto et al. 1991) which was followed up by the *Advanced Land Observing Satellite* (*ALOS*) *Phased Array type L-band Synthetic Aperture Radar* (*PALSAR*) *1* and *2* (1270 MHz) in 2002 and 2010, respectively (Rosenqvist et al. 2007; Kankaku et al. 2009; Shimada and Osawa 2012), the capability of spaceborne long-wavelength SAR has been widely exploited to monitor hidden subsurface geomorphologic features by amplitude image analysis, as shown in the work by, e.g., Paillou et al. (2007) and Paillou and Rosenqvist (2003).

Although there are dependences concerning mainly dielectric properties, Grandjean et al. (2001) calculated a penetration depth of airborne L-band SAR of up to 4 m using a two-layer subsurface scattering model and ground penetration radar over Pyle Dune, France. This is in some agreement with experiments conducted using SIR-A L-band radar (Schaber et al. 1986).

In this study, we aim to demonstrate the considerable potential by using SAR imaging not only for single-amplitude analysis of L-band SAR but also for making use of (1) multi-temporal/polarization amplitude and (2) polarimetric signatures that are acquired through multiple SAR imaging passes.

Different ALOS PALSAR-2 image data products such as amplitude, phase coherence and polarimetric information were processed to investigate the shallow subsurface of the Region of Interest (ROI) in more detail.

Polarimetric signatures such as amplitude ratios between HH, HV, VH and VV and their decomposition are likely related to the subsurface scattering and physical characteristics as shown in a sequence of studies by Gong et al. (2014) and Li et al. (2016) over Lop Nur lake employing ALOS PALSAR L-band polarimetric images, a field survey and a two-layer scattering model.

The anisotropy which is a polarimetric parameter that can be extracted by eigenvector–eigenvalue decomposition is a highly sensitive estimator of surface roughness. However, the studies by Liu et al. (2016) employing model-based target decompositions implied that subsurface properties such as the depth of a heterogeneous subsurface layer can contribute to the polarimetric signature, although the effects of the surface roughness are still more significant. Therefore, we expected subsurface volume scattering contributions especially considering the target area's condition where the surface is homogeneous and smooth as it is covered mostly the sand. Assuming such possibilities, the Pauli and eigenvector–eigenvalue decompositions (Cloude and Pottier 1996) were employed to potentially distinguish signatures from surface structures as well as surface conditions.

Although it is difficult to assess subsurface characteristics quantitatively using SAR/InSAR/polarimetric SAR techniques, interferometric/polarimetric signatures will support discriminating subsurface structures (e.g., Grandjean et al. 2001; Lasne et al. 2005; Touzi et al. 2009).

The ALOS PALSAR-2 data products used for this study are composed of *Spotlight* data with a ground resolution of 3 × 1 m in single polarization mode. The swath width is about 25 × 25 km. Additionally, we made use of *Stripmap* data in Ultra-Fine, High-Sensitive and Fine modes with ground resolutions of 3, 6 and 10 m, respectively. While data obtained in Ultra-Fine mode are available in single/dual polarization mode only, data from

High-Sensitive and Fine modes are available in single, dual and full polarization (see also Kankaku et al. 2009).

Among these, data obtained in (1) Stripmap Ultra-Fine mode with single polarization (2) high-sensitive dual model polarization (HH and HV) and (3) Fine mode full/dual polarization (HH and HV) were used for further investigation. In each case, amplitude images in dual and/or full polarization modes and polarimetric decomposition data from the full polarization mode were extracted and integrated into a spatial analysis platform. We aimed at investigating the extent and the origin of features in the region of interest (ROI) by fusing and comparing amplitude and polarimetric signatures from the dual polarization mode, as well as decompositions from full polarization modes from varying resolutions and under varying acquisition conditions.

Datasets for this work include processed yearly amplitude image mosaics obtained by PALSAR-2 (2015), for which RGB representations based on HH, HV and HH/HV polarization ratios were calculated. As penetration depth is a function of geologic materials and different polarization modes, the RGB band combination provides direct but qualitative information about different geological materials in the subsurface. ALOS PALSAR-1 (2008–2009–2010) amplitude mosaics were processed to potentially identify temporal surface changes over that time period.

Finally, Fine mode InSAR pairs as obtained on June 25, 2015, and October 29, 2015, were used to create a high-resolution HH, HV, HH/HV as RGB band combination in order to investigate the subsurface properties at higher spatial resolution.

These datasets were complemented by full polarization images from ALOS PALSAR-2 using the components from eigenvector–eigenvalue and Pauli decompositions in RGB representations and an Ultra-Fine mode amplitude mosaic map composed of images taken between July 2015 and February 2016 in HH polarization with a ground resolution of 6 m, in order to allow tracing surface and potentially subsurface features and structures in more detail.

We analyzed the Oasis impact structure by combining the ALOS PALSAR-1 and ALOS PALSAR-2 radar products described above with optical data and topography information. We integrated radiometrically, geometrically and atmospherically corrected multispectral Landsat 8 data in the optical and near-infrared wavelength range using a principal component (PC) representation and made use of a number of topographic products obtained from the USGS EarthExplorer platform. These include the photogrammetrically derived *Global Digital Elevation Model Version 2* (*GDEM V2*, NASA/JPL 2009) at a resolution of 1 arcsec (~30 m/px) from the *Advanced Spaceborne Thermal Emission and Reflection Radiometer* (*ASTER*) onboard NASA's Earth Observing System Terra satellite platform. Because of the ASTER GDEM's significant noise in desert areas, we made additional use of data from the *Shuttle Radar Topography Mission* (*SRTM*) with a resolution of 3 arcsec (~90 m/px, Farr et al. 2007). Gaps were filled by downsampled ASTER GDEM data.

Observations and discussion

The region of investigation covers parts of the Kufrah basin and foothills of the granite intrusions of the Jebel Al Awaynat (Jebel Uweinat). On Landsat ETM+ principal component representation, we can clearly identify the inner ring/central uplift (CU) of the Oasis impact structure (Fig. 1c, d) and circular arrangements of at least two other ring structures, which confirms earlier work by Koeberl et al. (2005b). Based on these data, the diameter of the impact structure can be estimated at 15–16 km on average, with a 8.1 km maximum in NNW–SSE direction. The Landsat-8 principal component analysis gives relatively high values for the first and third component resulting in dominantly red–blue units representing lower hillslope areas surrounding topographic heights and high-relief areas (Fig. 1c, d, IB and O). A relative dominance of the first and second principal component (orange) appears where paleoriver pathways leading from the SW to the NE—west of the Oasis impact structure—can be observed. These are generally only faintly visible in optical wavelength data. Finally, the Jebel Al Awynat in the eastern part of the ROI (J in Fig. 1c) is represented by a relative dominance of the third principal component (blue), while surrounding sandstone bedrock appears bluish greenish, with a higher relative dominance of the second principal component.

Using the 25 m ALOS PALSAR-2 amplitude image in HH and HV polarization modes (Fig. 2a–d) representing HH/HV/HH–HV as RGB, we can distinguish three major units in dark violet, brighter violet and yellow colors. Higher radar reflectance represented in HH/HH–HV (violet) is found in semi-consolidated and consolidated rocky material, where lower backscatter in HH/HH–HV polarization (dark violet) appears where erosional deposits and material related to fluvial erosion are abundant (label *pr* in Figs. 2c, d, 3a, b). Brighter colors are dominant where distinct bedrock layering (Fig. 2b–d) can be observed. Units in bright yellow are typically caused by strong backscatter and HV polarization modes with HH/HV represented as blue approaches zero. They clearly show and delineate consolidated material and bedrock exposed at the surface. As they are clearly distinguishable from the sand-covered layered bedrock, they help to trace the outline of the Oasis impact crater structure.

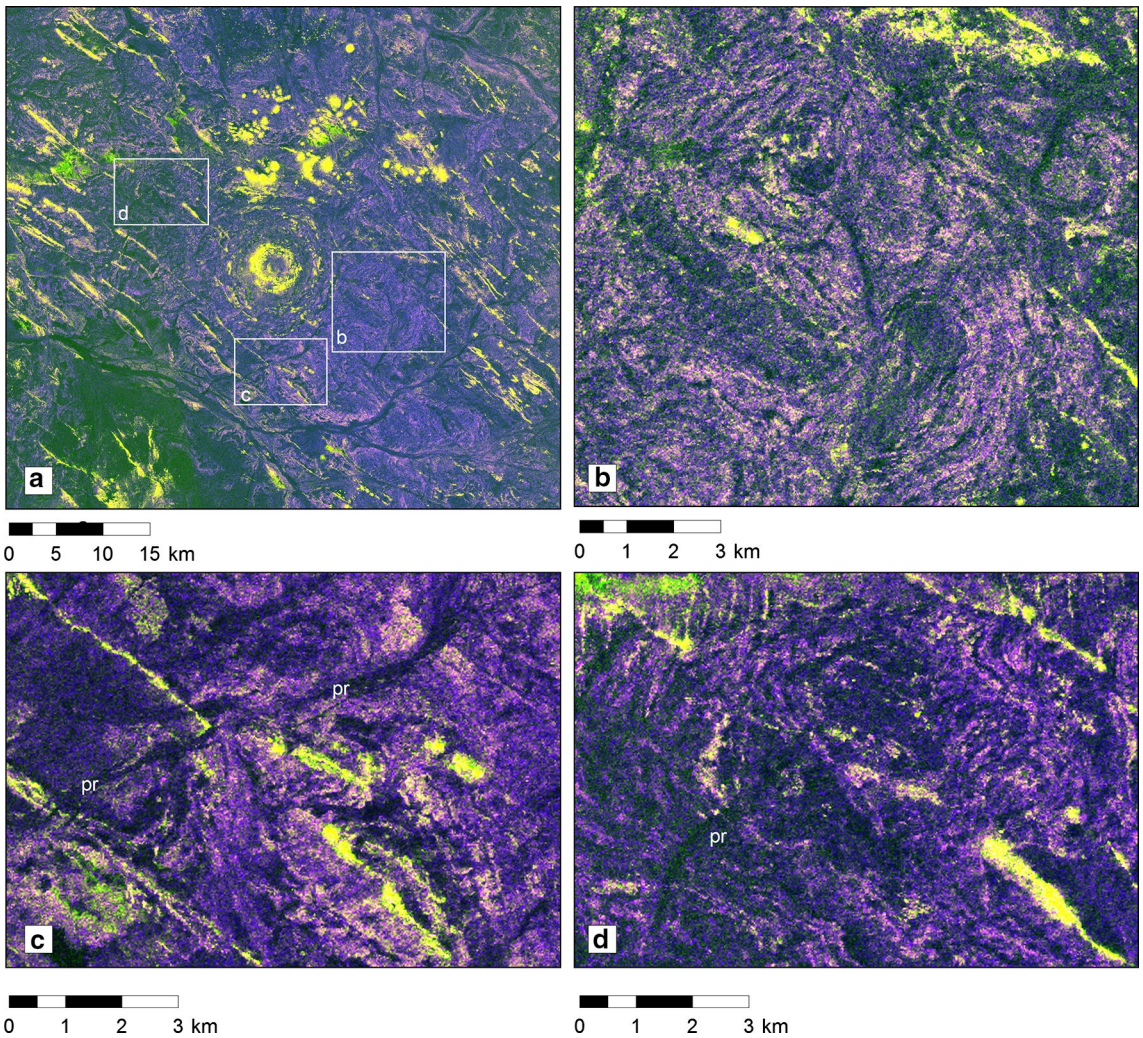

Fig. 2 ALOS PALSAR-2 polarimetric amplitude RGB composite in HH/HV/HH–HV polarization modes (27 m/px). **a** Is a broader overview with the Oasis structure in the image center. *Purple colors* represent high (on a relative scale) radar reflectance in HH polarization, *yellow colors* show high reflectance values also in HV polarization indicating exposed bedrock units; center of impact structure located at 24°24′E, 24°34′N. **b** Insights into the near-subsurface structure with pronounced horizontal layering not visible in Landsat ETM image data (center at 24°31′E, 24°32′N). **c** A paleoriver system (*pr*) is clearly visible and distinct in polarimetric data but diffuse in optical image data. Possible folding with fold axes in NW–SE direction for elongated ridges in the southern part (center at 24°24′E, 24°28′N). **d** Complex layering and paleodrainage (pr, center at 24°17′E, 24°39′N)

A paleoriver system delineates the inner ring structure (Figs. 2c, d, 3a, b, 4 and 5) and intersects distal parts of the outer ring; it, therefore, postdates the impact event. Abundant elongated bedrock outcrops striking NW–SE, as well as the inselbergs north of the Oasis impact structure, seem relatively pristine and undisturbed at this scale. This was also suggested by Underwood and Fisk (1980) as referenced in Koeberl et al. (2005b). On radar datasets, we derive an average diameter of 15.6 km for the impact structure, for this erosional level, but we cannot rule out that its pre-erosional size was larger. However, given the arrangement of the delineating paleoriver system clearly delineating the structure, it must have been eroded to this level when the *Messinian Salinity Crisis* (*MSC*) took place some 5.5 Myr ago (e.g., Gautier et al. 1994).

The polarimetric decompositions performed on the Oasis impact crater observations (Fig. 3a) using the Pauli decomposition (Fig. 3b) and the entropy–alpha–anisotropy decomposition (Fig. 3c) both provide qualitative information for image interpretation and are useful in particular for the differentiation between unconsolidated sediment cover and bedrock units, and some of the larger-scale structural inventory. Considerable noise in

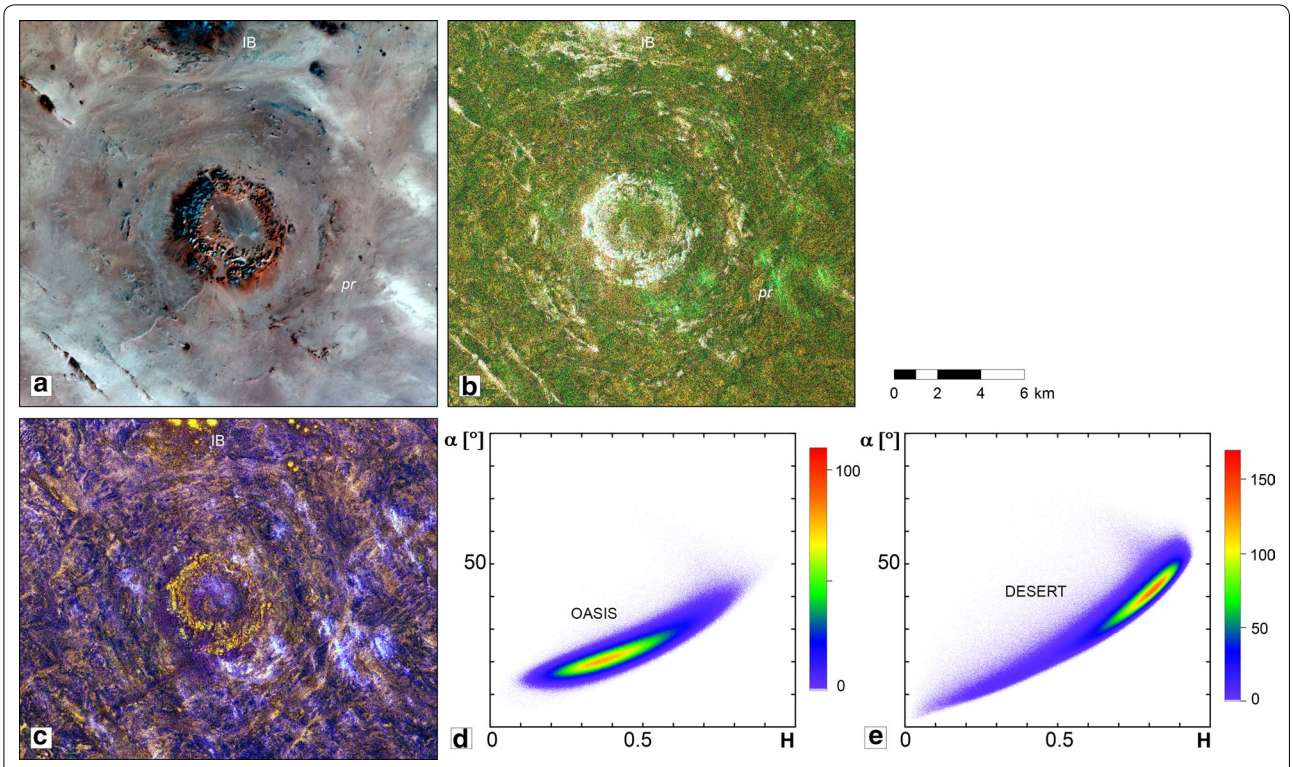

Fig. 3 **a** Landsat 321 as RGB overview of the Oasis impact structure with its inner and outer ring as reference (30 m/px). **b**, **c** ALOS PALSAR-2 derived data representations (25 m/px). **b** Polarimetric Pauli decomposition with even-bounce/dihedral rotated/odd-bounce components represented as RGB. **c** Entropy (H)–alpha (α)–anisotropy (A) decomposition represented as RGB. The center of the impact structure is located at 24°24′E, 24°34′N. **d**, **e** H–α-plane scatter plot for the Oasis impact structure (**d**) and a region covering the Libyan Desert centered at 25°03′N, 21°55′E (**e**)

the Pauli decomposition allows mapping of major units only, while the entropy–alpha–anisotropy decomposition allows observing the overarching structural regime as indicated in Fig. 3c. The contribution of subsurface scattering in the Oasis area is negligible based on the point distribution in H/α-plane (e.g., Lee and Pottier 2009), as we find a maximum in the low-H and low-α range (Fig. 3d) indicating dominant low and random surface scattering (Lee and Pottier 2009). For other areas in the Libyan Desert, medium entropy of both surface and volume scattering terms seems dominant (Fig. 3e).

Most valuable for interpretation purposes of fine-scaled structures is the ALOS PALSAR-2 radar image taken in Ultra-Fine mode with a resolution of 3 m/px (Fig. 4). Due to considerable noise it was filtered and resampled to 10 m. It provides the backscatter amplitude in HH polarization and is therefore similar to the data presented in Fig. 2a–d (red component). The potential to map the structural and depositional inventory (faults, folds, layering along with thicknesses), as well as the potential to easily differentiate between consolidated and unconsolidated material in the near (sub-) surface, remains identical (Fig. 5). However, the high-resolution image poses some challenges, in particular in convoluted areas near the inner ring where strata are more chaotically arranged and postimpact fluvial erosion overprints the original settings [see streamlined island (sb) in Fig. 4b]. The returned radar backscatter is composed of surface and near-subsurface reflectance. As shown in Fig. 4c, d, the exposed inner ring shows distinct layering (Fig. 4c), whereas the northern inselbergs (Fig. 4d) appear not layered at this image scale. The layering attitude, however, cannot be quantified due to radar foreshortening effects, but it is considered relatively steep in the inner ring structure. In Fig. 4d, the contact between impact-deformed bedrock with potential folding and undisturbed units of different origin just to the north is exposed, which potentially helps to delineate the impact structure as it is observed today. Using these boundaries, we estimate a diameter of 15.6 ± 0.3 km depending on the location of measurement profile as the overall shape of the outermost ring is slightly asymmetric, which could be caused by erosional effects rather than being due to a specific angle of impact.

Based on observations on amplitude data in different polarization modes, we observe three different bedrock units (Figs. 2a–d, 5).

The first unit (ring remnant unit in Fig. 5) is composed of numerous exposed sub-circular or elongated

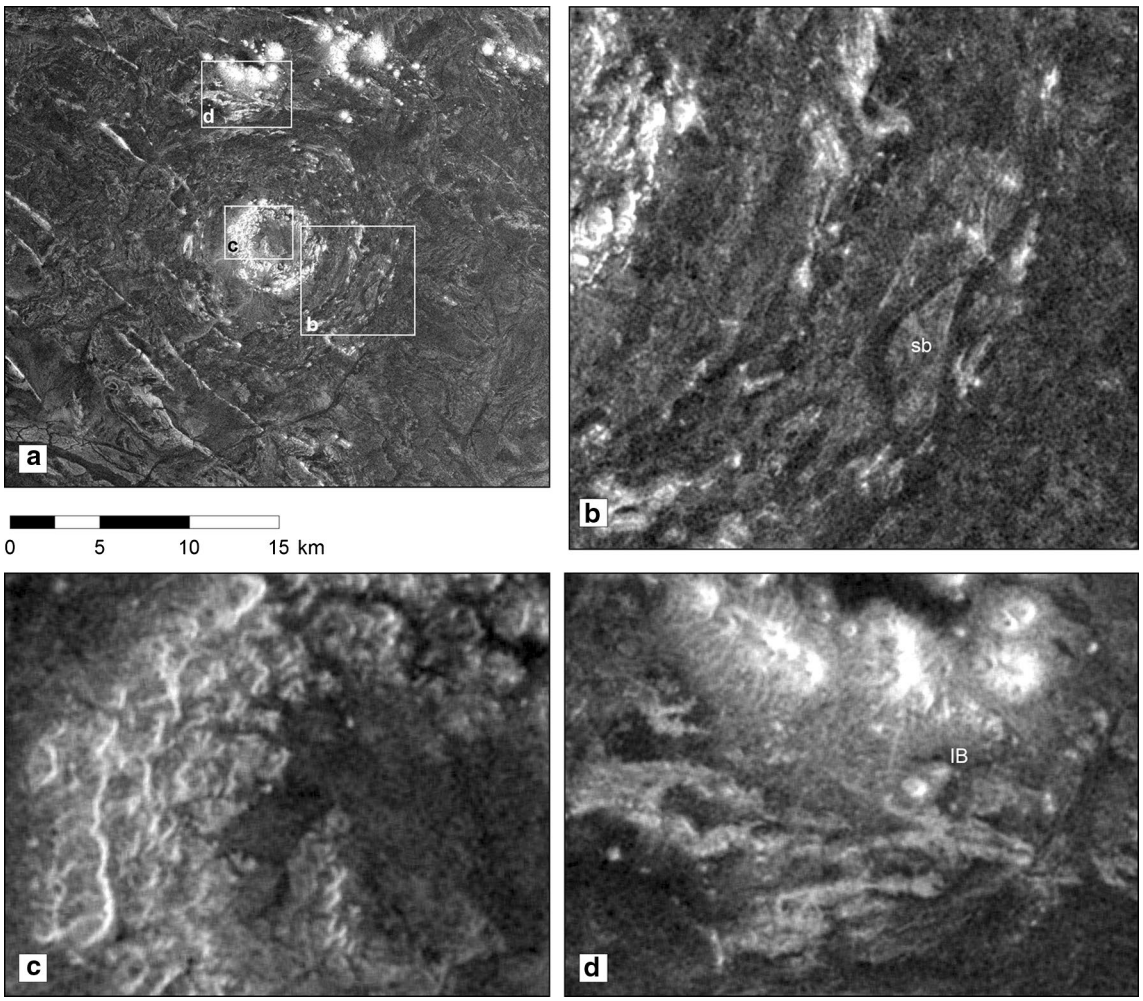

Fig. 4 **a** Overview of the ALOS PALSAR-2 amplitude image in Ultra-Fine mode with a resolution of 3 m/px. HH polarization (filtered and resampled to reduce noise). The center of the impact structure is located at 24°24′E, 24°34′N; **b** complex arrangement of impact-related layering and fluvial overprint, center at 24°27′E, 24°33′N. **c** Layering at the inner ring (center at 24°24′E, 24°34′N) and **d** layering exposed north of the Oasis impact crater (center at 24°24′E, 24°39′N)

features that are arranged in a circular way around what is interpreted as the central uplift, including the inner ring (Fig. 4). The primary middle ring has a diameter of approximately 4.6 km but seems to be variable as also stressed by Koeberl et al. (2005b). A second middle ring with a diameter of 10.9 km, on average, is topographically less prominent but can be traced by the distribution of surface rock units. Units of the outermost ring are exposed at a distance of up to 8.1 km from the center (Fig. 4). These units border isolated circular bedrock units described as second unit below. Based on radar amplitude data, the outer units seem to be highly inclined (Figs. 2 and 4) and partially folded (Fig. 4b).

The second unit (clustered remnant unit in Fig. 5) consists of isolated and clustered, partly coalescing, circular inselbergs in the northern part of the ROI, north of the Oasis impact structure (IB in Figs. 1d, 2a, and southern parts in Fig. 5). The distribution does not seem to follow any particular direction but features seem to be grouped into five major clusters. They have been described as *clastic plugs* by Underwood and Fisk (1980) and were discussed later by Koeberl et al. (2005b) and interpreted as potential remains of fold cores. Whether they are associated with the Oasis impact event remains open. Based on an analysis of the spectrally relatively limited Landsat sensor data, we cannot distinguish lithologies of ring units from units forming these remnant knobs. Both origins discussed in the literature would cause the same spectral signal, even at higher spatial and spectral resolution, and are therefore conceivable.

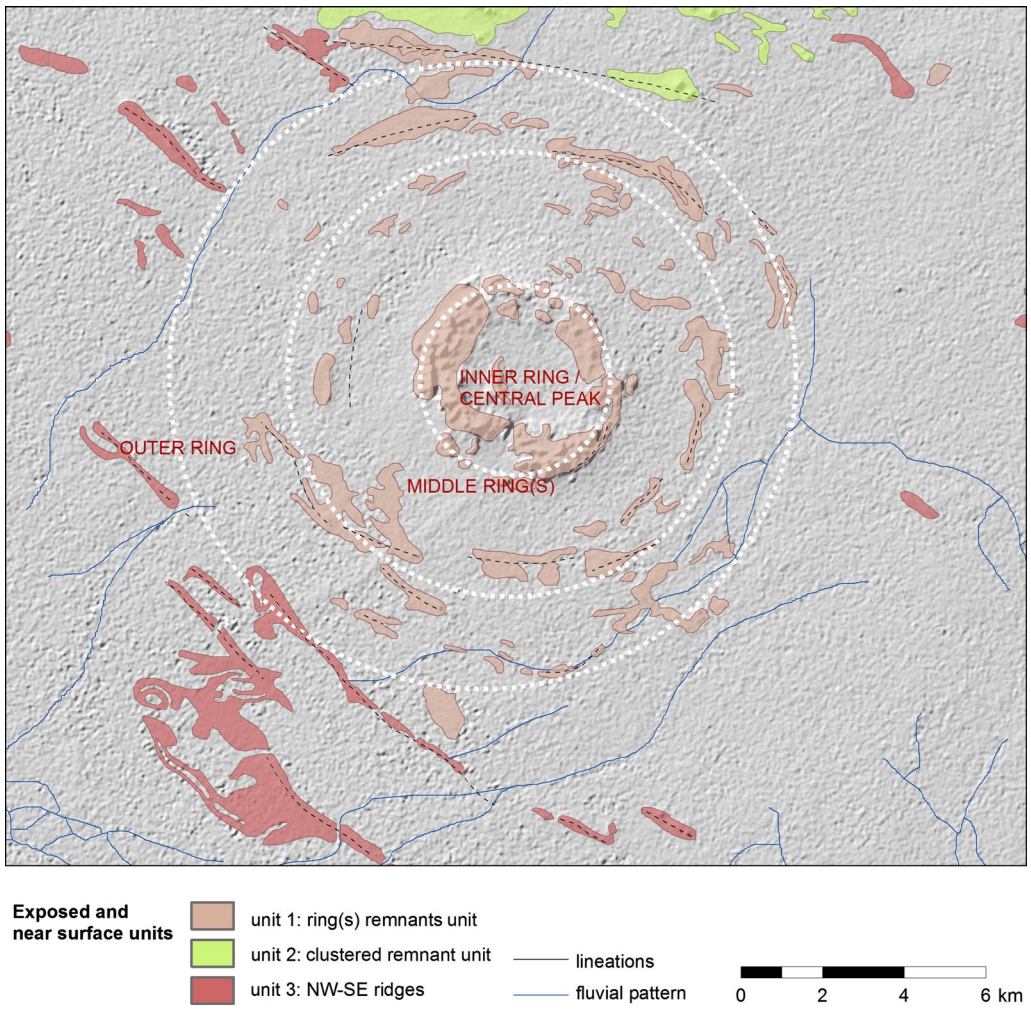

Fig. 5 Sketch map with extents of geomorphologic units and paleodrainage system based on highest resolution ALOS PALSAR-2 polarimetric data. The center of the impact structure is located at 24°24′E, 24°34′N

The third unit (NW–SE ridges in Fig. 5) is relatively common across the area and can be traced toward the east and west of the ROI. In particular to the west, these features extend for several tens to hundreds of kilometers and are consequently not impact-related. The unit consists of straight and well-defined ridges with a segment length of tens of meters to kilometers. They are distributed in NW–SW direction and were cut by the impact. Spectrally, these units cannot be distinguished from other rock units in the ROI, which might suggest that they are eroded remnants of older Kufrah basin units. Their alignment corresponds to the general alignment of subbasins in the Kufrah basin (Pachur and Altmann 2006), which might imply a dominant tectonic control. Circulation and rise of alcalic solutions along fractures and faults might have caused a higher resistance to erosion, although other mechanisms seem to be conceivable as well (Pachur and Altmann 2006: 395). The origin of these features remains unknown, and although they have been labeled by Koeberl et al. (2005b: 172), they have not been described in any detail.

Interpretations and conclusions

Little is known about the Oasis impact structure, as the detailed structural inventory, its exact spatial extent and formation age are not well constrained. Field studies are hampered by the political situation (see also description in Koeberl et al. 2005b) and currently, remote sensing studies remain the only way to shed new light on some of the open questions. We here studied the Oasis impact structure using optical and radar data, and derived products from ALOS PALSAR-2.

Based on the available radar data products, it is not possible to distinguish different lithologies in the larger area but it is possible to clearly separate bedrock units from unconsolidated materials based on the respective radar backscatter with high radar reflectance for bedrock units and low reflectance for unconsolidated material. H/α-plane analysis showed that the radar backscatter is derived from surface units mainly and that the subsurface component is of minor relevance. The combination of various primary and secondary radar datasets helped to look into the overall geologic and geomorphologic settings in more detail than currently freely available optical image data could provide.

In particular, Ultra-Fine resolution polarimetric ALOS PALSAR-2 data are helpful for more confident structural and geologic mapping, and the radar data form a useful addition for investigating prospective impact structures in remote environments. Using high-resolution Ultra-Fine radar imaging (3 m/px), we can estimate the diameter of the Oasis impact structure at 15.6 ± 0.5 km at the current erosion level. This is supported not only by the sub-circular arrangement of structural units but also by the presence of postimpact paleoriver systems delineating and partially crossing the ring structures. There is a slight ring asymmetry which might be caused by erosional effects rather than oblique impacts (see also Gibson et al. 2011).

Based on radar and optical imagery, we cannot observe any deformation outside the mapped outer ring, in particular as the remnant unit in the north (unit 2 in Fig. 5) seems completely undisturbed. In the south, elongated remnant ridges (unit 3) delineate what we interpret the maximum extent of the Oasis impact structure. Both units are in consistent agreement, although we cannot rule out a much larger size as discussed briefly in the literature (Gibson et al. 2011).

At this stage, we cannot provide much detailed insights into the impact age that was determined to be 90–120 Myr as upper maximum by Gibson et al. (2011). Given that the observed paleohydraulic network formed after the impact event, the impact must have occurred before the MSC and therefore formed before 5.5 Myr ago. The impact also truncates NW–SE ridges that could be considered remnants of a Paleozoic basement (Pachur and Altmann 2006).

For structural and geomorphic mapping, polarimetric ALOS PALSAR-2 data can help significantly if the settings are not too complex. The function of backscatter depends largely on material properties and the mixed return signal rules out any quantitative assessment at the time of writing. In geologically complex areas with significant overprint, it might become impossible to interpret the structural settings properly.

We believe that for canopy-free desert areas the analysis of SAR data would significantly improve the possibility to interpret the structure and geologic settings of impact structures, in particular if they are heavily eroded or covered by material, despite relatively high demands on data processing. In combination with field observation and additional remote sensing datasets from optical sensors, radar data analysis provides a broad range of derived data products that might help to diminish false detections of impact structures.

Authors' contributions

SvG prepared and wrote the manuscript, performed data interpretation and provided the overall storyline. JRK defined the initial research target, acquired and processed radar data, and contributed the section on methodological aspects. YSC and JYK provided support for data interpretation and manuscript development, and contributed substantially in discussions on the manuscript's contents. All authors read and approved the final manuscript.

Acknowledgements

This research was supported by Korean National Research Foundation (Grant No. 2013078206) and by the Korean Brain Pool Program. ALOS image data are kindly provided by JAXA 6th ALOS scheme P1488002. We are grateful for thorough reviews from Wolf Uwe Reimold and an anonymous reviewer who have helped to substantially improve this manuscript.

Competing interests

The authors declare that they have no competing interests.

Received: 27 October 2016 Accepted: 17 February 2017
Published online: 27 February 2017

References

Abdelsalam M, Robinson C, El-Baz F, Stern R (2000) Applications of orbital imaging radar for geologic studies in arid regions: the Sharan Testimony. Photogramm Eng Remote Sens 66(6):717–726

Abels A, Zumsprekel H, Bischoff L (2000) Basic remote sensing signatures of large, deeply eroded impact structures. In: Gilmour I, Koeberl C (eds) Impacts and the early earth, vol 91., Lecture notes in earth sciencesSpringer, Berlin, pp 309–326

Adams R, Brown W, Culbert T (1981) Radar mapping, archeology, and ancient maya land use. Science 213:1457–1463

Barr FT, Walker BR (1973) Late tertiary channel system in northern Libya and its implications on Mediterranean Sea level changes. In: Ryan WBF, Hsü KJ, Cita MB, Dumitrica P, Lort JM, Maync W, Nesteroff WD, Pautot G, Stradner H, Wezel FC, Kaneps AG (eds) Initial reports of the Deep Sea Drilling Project, covering Leg 13 of the cruises of the drilling vessel Glomar Challenger Lisbon, Portugal to Lisbon, Portugal, pp 1244–1251. doi:10.2973/dsdp.proc.13.144-4.1973

Berlin G, Tarabzouni M, Al-Naser A, Sheikho K, Larson R (1986) SIRB subsurface imaging of a sand-buried landscape: Al Labbah Plateau, Saudi Arabia. IEEE Trans Geosci Remote Sens 4:595–601

Blom R, Crippen R, Elachi C (1984) Detection of subsurface features in SEASAT radar images of Means Valley, Mojave Desert, California. Geology 12:346–349

Buchner E, Schmieder M (2007) Mousso structure: a deeply eroded, medium-sized, complex impact crater in northern Chad? J Afr Earth Sci 49(3):71–78

Cigolini C, Di Martino M, Laiolo M, Coppola D, Rosetti P, Morelli M (2012) Endogenous and nonimpact origin of the Arkenu circular structures (al-Kufrah basin—SE Libya). Meteorit Planet Sci 47(11):1772–1788. doi:10.1111/maps.12012

Cloude SR, Pottier E (1996) A review of target decomposition theorems in radar polarimetry. IEEE Trans Geosci Remote Sens 34(2):498–518

Crósta AP, Reimold WU (2015) Impact craters in South America, by Acevedo RD, Rocca MCL, Ponce JF, and Stinco SG Heidelberg: Springer, 2015. 104 p, Springer Briefs in Earth Sciences: South America and the Southern Hemisphere. Meteorit Planet Sci 51(5):996–999

Daneshvar MRM (2015) Remote sensing analysis for the possible impact structure of Lakhcak Crater in southern Afghanistan. Appl Geomat 7:275–282. doi:10.1007/s12518-015-0164-1

Drake NA, El-Hawat AS, Turner P, Armitage SJ, Salem MJ, White KH, McLaren S (2008) Palaeohydrology of the Fazzan Basin and surrounding regions: the last 7 million years. Palaeogeogr Palaeoclimatol Palaeoecol 263:131–145

Elachi JC, Roth LE, Schaber GG (1984) Spaceborne radar subsurface imaging in hyperarid regions. IEEE Trans Geosci Remote Sens 4:383–388

El-Baz F, Ghoneim E (2007) Largest crater shape in the Great Sahara revealed by multi-spectral images and radar data. Int J Remote Sens 28(2):451–458

Farr TG, Rosen PA, Caro E, Crippen R, Duren R, Hensley S, Kobrick M, Paller M, Rodriguez E, Roth L, Seal D, Shaffer S, Shimada J, Umland J, Werner M, Oskin M, Burbank D, Alsdorf D (2007) The shuttle radar topography mission. Rev Geophys. doi:10.1029/2005RG000183

Folco L, Di Martino M, El Barkooky A, D'Orazio M, Lethy A, Urbini S, Nicolosi I, Hafez M, Cordier C, van Ginneken M, Zeoli A, Radwa AM, El Khrepy S, El Gabry M, Gomaa M, Barakat AA, Serra R, El Sharkawi M (2010) The kamil crater in Egypt. Science 329(5993):804

Folco L, Di Martino M, El Barkooky A, D'Orazio M, Lethy A, Urbini S, Nicolosi I, Hafez M, Cordier C, van Ginneken M, Zeoli A, Radwa AM, El Khrepy S, El Gabry M, Gomaa M, Barakat AA, Serra R, El Sharkawi M (2011) Kamil crater (Egypt): ground truth for small-scale meteorite impacts on Earth. Geology 39(2):179–182

French BM, Koeberl C (2010) The convincing identification of terrestrial meteorite impact structures: what works, what doesn't, and why. Earth Sci Rev 98:123–170

French BM, Underwood JR Jr, Fisk EP (1972) Shock-metamorphic effects in two new Libyan impact structures. Geol Soc Am 4:510–511

French BM, Underwood JR, Fisk EP (1974) Shock metamorphic features in two meteorite impact structures, Southeastern Libya. Geol Soc Am Bull 85:1425–1428

Garvin JB, Schnetzler CC, Grieve RAF (1992) Characteristics of large terrestrial impact structures as revealed by remote sensing studies. Tectonophysics 216:45–62

Gautier F, Clauzon G, Suc JP, Cravatte J, Violanti D (1994) Age and duration of the Messinian salinity crisis. C R Acad Sci Paris (IIA) 318:1103–1109

Gibson RL, Reimold WU, Baegi M, Crosta AP, Shbeli E, Eshwedi A (2011) The Oasis structure, southeastern Libya: new constraints on size, age and mechanism of formation. In: Lunar and planetary science conference abstracts, vol 42. #1024, Houston

Gong H, Shao Y, Zhang T, Liu L, Gao Z (2014) Scattering mechanisms for the "Ear" feature of Lop Nur lake basin. Remote Sens 6(5):4546–4562

Grandjean G, Paillou P, Dubois-Fernandez P, August-Bernex T, Baghdadi NN, Achache J (2001) Subsurface structures detection by combining L-band polarimetric SAR and GPR data: example of the Pyla Dune (France). IEEE Trans Geosci Remote Sens 39(6):1245–1258

Griffin DL (2002) Aridity and humidity: two aspects of the late Miocene climate of North Africa and the Mediterranean. Palaeogeogr Palaeoclimatol Palaeoecol 182:65–91

Griffin DL (2006) The late Neogene Sahabi rivers of the Sahara and their climatic and environmental implications for the Chad basin. J Geol Soc Lond 163:905–921

Kankaku Y, Osawa Y, Suzuki S, Watanabe T (2009) The overview of the L-band SAR onboard ALOS-2. In: Proceedings of the progress in electromagnetics research symposium. 18–21 Aug

Koeberl C (2004) Remote sensing studies of impact craters: How to be sure? C R Geosci 336:959–961

Koeberl C, Reimold WU, Cooper G, Cowan D, Vincent P (2005a) Aorounga and Gweni Fada impact structures, Chad: remote sensing, petrography, and geochemistry of target rocks. Meteorit Planet Sci 40:1–17

Koeberl C, Reimold WU, Plescia J (2005b) BP and Oasis impact structures, Libya: remote sensing and field studies. In: Koeberl C, Henkel H (eds) Impact tectonics. Springer, Berlin, pp 161–190

Kohman TP, Lowman PD, Abdelkhalek ML (1967) Space and aerial photography of the Libyan Desert glass area. In: Proceedings of the 30th annual meteoritical society meeting. Moffett Field

Lasne Y, Paillou P, Ruffié G, Crapeau M (2005) Effect of multiple scattering on the phase signature of wet subsurface structures: applications to polarimetric L-and C-band SAR. IEEE Trans Geosci Remote Sens 43(8):1716–1726

Lee JS, Pottier E (2009) Polarimetric radar imaging. CRC Press, Boca Raton

Li B, Gong H, Shao Y, Li L, Wang L, Liu C, Xie K (2016) The consistency between Na content distribution at the subsurface and the lake body's movement in Lop Nur. Int J Digit Earth 9(7):662–675

Liu CA, Gong H, Shao Y, Yang Z, Liu L, Geng Y (2016) Recognition of salt crust types by means of PolSAR to reflect the fluctuation processes of an ancient lake in Lop Nur. Remote Sens Environ 175:148–157

Mader M (2015) The Mistastin Lake impact structure as a terrestrial analogue site for lunar science and exploration. Electronic Thesis and Dissertation Repository. Paper 3485. The University of Western Ontario. http://ir.lib.uwo.ca/etd/3485

Martin AJ (1969) Possible impact structure in southern Cyrenaica, Libya. Nature 223:940–941

McCauley JF, Schaber GG, Breed CS, Grolier MJ, Haynes CV, Issawi B, Elachi C, Blom R (1982) Subsurface valleys and geoarchaeology of the eastern Sahara revealed by Shuttle Radar. Science 218:1004–1020

McHone JF, Greeley R, Williams KK, Blumberg DG, Kuzmin RO (2002) Space shuttle observations of terrestrial impact structures using SIR-C and X-SAR radars. Meteorit Planet Sci 37:407–420

Michaelski JR, Bleacher JE (2013) Supervolcanoes within an ancient volcanic province in Arabia Terra, Mars. Nature 502:47–52. doi:10.1038/nature12482

NASA JPL (2009) ASTER global digital elevation model. NASA JPL. doi:10.5067/ASTER/ASTGTM.002

Nemoto Y et al (1991) Japanese earth resources satellite-1 synthetic aperture radar. Proc IEEE 79(6):800–809

Orti L, Di Martino M, Morelli M, Cigolini C, Pandeli E, Buzzigoli A (2008) Non-impact origin of the crater-like structures in the Gilf Kebir area (Egypt); implications for the geology of eastern Sahara. Meteorit Planet Sci 43(10):1629–1639

Pachur HJ, Altmann N (2006) Die Ostsahara im Spätquartär. Springer, Berlin, p 662

Paillou P, Rosenqvist A (2003) A JERS-1 radar mosaic for subsurface geology mapping in East Sahara. In: IEEE international geoscience and remote sensing symposium

Paillou P, Rosenqvist A, Malezieux J-M, Reynard B, Farr T, Heggy E, Papagiannis M (2003) Discovery of a double impact crater in Libya: the astrobleme of Arkenu. C R Geosci 335:1059–1069

Paillou P, Lasne Y, Heggy E, Malézieux JM, Ruffié G (2006a) A study of P-band synthetic aperture radar applicability and performance for Mars exploration: imaging subsurface geology and detecting shallow moisture. J Geophys Res Planets 111(E6). doi:10.1029/2005JE002528

Paillou P, Reynard B, Malézieux JM, Dejax J, Heggy E, Rochette P, Reimold WU, Michel P, Baratoux D, Razin P, Colin JP (2006b) An extended field of crater-shaped structures in the Gilf Kebir region, Egypt: observations and hypotheses about their origin. J Afr Earth Sci 46:281–299

Paillou P, Lopez S, Lasne Y, Rosenqvist A, Farr T (2007) Mapping subsurface geology in Arid Africa using L-band SAR. In: IEEE international geoscience and remote sensing symposium

Paillou P, Schuster M, Tooth S, Farr T, Rosenqvist A, Lopez S, Malezieux J (2009) Mapping of a major paleodrainage system in eastern Libya using orbital imaging radar: the Kufrah River. Earth Planet Sci Lett 277(3–4):327–333. doi:10.1016/j.epsl.2008.10.029

Paillou P, Tooth S, Lopez S (2013) The Kufrah paleodrainage system in Libya: a past connection to the Mediterranean Sea? C R Geosci 344(8):406–414

Papagiannis MD (1989) Photographs from geostationary satellites indicate the possible existence of a huge 300 km impact crater in the Bohemian region of Czechoslovakia. Meteoritics 24:313

Pati JK, Reimold WU (2007) Impact cratering: fundamental process in geosciences and planetary science. J Earth Syst Sci 116(2):81–89

Reimold WU (2007) The impact crater bandwagon (some problems with the terrestrial impact cratering record). Meteorit Planet Sci 42(9):1467–1472

Reimold WU, Koeberl C (2014) Impact structures in Africa: a review. J Afr Earth Sci 93:57–175

Reimold WU, Gibson RL, Koeberl C (2013) Comment on: searching for giant, ancient impact structures on Earth—the Mesoarchaean Maniitsoq structure, West Greenland. Earth Planet Sci Lett 369–370:333–335

Reimold WU, Ferrière L, Deutsch A, Koeberl C (2014) Impact controversies: impact recognition criteria and related issues. Meteorit Planet Sci 49(5):723

Richards JA (2009) Remote sensing with imaging radar. Signals and communication technology. Springer, New York

Rosenqvist A, Shimada M, Ito N, Watanabe M (2007) ALOS PALSAR: a pathfinder mission for global-scale monitoring of the environment. IEEE Trans Geosci Remote Sens 45(11):3307–3316

Schaber GG, McCauley JF, Breed CS, Olhoeft GR (1986) Shuttle imaging radar: physical controls on signal penetration and subsurface scattering in the eastern Sahara. IEEE Trans Geosci Remote Sens 24:603–623

Schmieder M, Buchner E, Le Heron P (2008) The Jebel Hadid structure (Al Kufrah Basin, SE Libya): a possible impact structure and potential hydrocarbon trap? J Asian Earth Sci 64:58–76

Schmieder M, Seyfried H, Gerel O (2013) The circular Uneged Uul structure (East Gobi Basin, Mongolia): geomorphic and structural evidence for meteorite impact into an unconsolidated coarse-clastic target? J Asian Earth Sci 64:58–76

Shimada M, Osawa Y (2012) ALOS-2 science program and high resolution SAR applications. Proc SPIE 8528:852812. doi:10.1117/12.979379

Smith SK, Grieve RAF, Harris JR, Singhroy V (2014) The utilization of RADARSAT-1 imagery for the characterization of terrestrial impact landforms. Can J Remote Sens 25(3):1999

Touzi R, Deschamps A, Rother G (2009) Phase of target scattering for wetland characterization using polarimetric C-band SAR. IEEE Trans Geosci Remote Sens 47(9):3241–3261

Underwood JR, Fisk EP (1980) Meteorite impact structures, southeast Libya. In: Salem MJ, Busrewil MT (eds.) The geology of libya, proceedings, Symposium 1978. London, pp 893–900

van Gasselt S, Hauber E, Neukum G (2007) Cold-climate modification of Martian landscapes: a case study of a spatulate debris landform in the Hellas Montes Region, Mars. J Geophys Res 112:E09006. doi:10.1029/2006JE002842

Wagner R, Reimold WU, Brandt D (2002) Bosumtwi impact crater, Ghana: a remote sensing investigation. In: Plado J, Pesonen LJ (eds) Meteorite impacts in precambrian shields, impact studies, vol 2. Springer, Heidelberg, pp 189–210